

Article

Thermal Expansion and Phase Transformation up to 1200 °C of Metastable Aluminas Produced by Flame Spraying

Tilo Zienert  and Christos Georgios Aneziris

Institute of Ceramics, Refractories and Composite Materials, TU Bergakademie Freiberg, Agricolastr. 17, 09599 Freiberg, Germany; aneziris@ikfvw.tu-freiberg.de

* Correspondence: tilo.zienert@licoo.de or tilo.zienert@ikfvw.tu-freiberg.de; Tel.: +49-3731-39-1546

Abstract: The transition aluminas δ_1 and the cubic, non-spinel-type η - Al_2O_3 were detected in addition to α - Al_2O_3 in flame-sprayed material. Their transitions from room temperature up to 1200 °C were investigated by high-temperature XRD measurements. Structural changes with time and temperature were observed for all transition aluminas (η -, δ_1 - and θ - Al_2O_3). The phases followed the expected transition sequence of $\eta \rightarrow \delta_1 \rightarrow \theta \rightarrow \alpha$ and showed mainly linear, temperature-independent transition rates. Based on the determined thermal expansion of the phases, it is proposed that the metastable transitions are at least partly mechanically induced. In addition, a second-order phase transition from $\eta \rightarrow \theta$ might be indicated around 1050–1075 °C by the determined trends of density.

Keywords: transition aluminas; thermal expansion; phase transformations; flame-spraying



Citation: Zienert, T.; Aneziris, C.G. Thermal Expansion and Phase Transformation up to 1200 °C of Metastable Aluminas Produced by Flame Spraying. *Crystals* **2023**, *13*, 743. <https://doi.org/10.3390/cryst13050743>

Academic Editors: Karolina Siedliska, Kamila Komędera and Raffaello Mazzaro

Received: 3 April 2023
Revised: 20 April 2023
Accepted: 24 April 2023
Published: 29 April 2023



Copyright: © 2023 by the authors. Licensee MDPI, Basel, Switzerland. This article is an open access article distributed under the terms and conditions of the Creative Commons Attribution (CC BY) license (<https://creativecommons.org/licenses/by/4.0/>).

1. Introduction

The transition aluminas γ , δ and θ are of interest for catalytic applications due to their special surface properties [1] depending on their structural disorder, surface area and their thermodynamic stability [2]. These aluminas are typically derived from the heat treatment of boehmite and form the general transition sequence of $\gamma \rightarrow \delta \rightarrow \theta \rightarrow \alpha$ on heating with the final formation of α - Al_2O_3 at temperatures above 1200 °C [3]. Seeding with α - Al_2O_3 lowers the activation energy and increases the transition rate of α - Al_2O_3 formation from the transition aluminas [4]. Plasma- or flame-sprayed alumina coatings and protective layers [3,5–7] are another source of transition aluminas that show the same general transformation sequence. Intermediate aluminas are structurally based on a slightly distorted cubic closed-packed sublattice of oxygen ions [8] containing structurally ordered vacancies, stacking faults and antiphase boundaries [8–10]. Besides, structural defects and their thermodynamic consequences for the nucleation and growth of ordered domains in the γ matrix, phase transitions and surface properties are also affected by the morphology of the respective crystals [1,11–13], leading to, e.g., a direct $\gamma \rightarrow \theta$ transition [1]. Typically, the transition from one intermediate state to the next is not marked by a certain transition temperature but a transition range [14,15], which shows time dependence [16,17] and structural ordering [18,19].

It has been reported that in case of quenched alumina melts, the formed γ -alumina is not of the cubic spinel-type but it forms a cubic η variant, where metallic ions are also present at non-spinel positions [20]. Non-spinel-type γ - Al_2O_3 is energetically more stable than the spinel-type, as shown by first-principle calculations [21]. The occupation of non-spinel sites in γ - Al_2O_3 is related to pore size/surface area [22]. At least for the boehmite-derived γ -aluminas, a tetragonal distortion is frequently reported, e.g., [16,23,24].

The structure of δ - Al_2O_3 was an open question for a long time [9], until its nature was recently revealed with the development of several structural models [25]. In boehmite-based samples, δ -alumina was found to be formed by at least five different structures that were named δ_1 to δ_5 [17,25,26], showing complex intergrown microstructures [27].

Coarse-grained refractory composites based on Nb–Al₂O₃ or Ta–Al₂O₃ systems are promising materials for high-temperature applications (1500–1800 °C) with a metallurgical background [28]. Despite their good mechanical and functional (electrical and thermal conductivity) properties [29,30], these compounds are susceptible to oxidation at temperatures above 400 °C [31], which must be prevented by use in oxygen-containing environments. Alumina-based flame-sprayed coatings show very good thermal-shock resistance even at temperature gradients higher than 1000 K [32]. Such coatings are also promising candidates for oxygen protecting layers. On heating, the phase transitions of metastable aluminas could be a source of thermal stresses and corresponding crack initiation in flame-sprayed coatings, which could lead to the formation of pores and spalling effects and could be prevented by a regulated heat treatment. Therefore, the aim of this work was to investigate the thermal expansion of transition aluminas present after flame spraying between room temperature and 1200 °C using high-temperature powder X-ray diffraction measurements. The thermal expansion of α -, η -, δ_1 - and θ -Al₂O₃ was studied and the possible consequences of inducing phase transitions are discussed.

2. Materials and Methods

2.1. Sample Preparation

Specimens were fabricated via flame spraying on graphite pins ($d = 15$ mm) using a MasterJet flame-spray gun (Saint-Gobain, Avignon, France). The feedstock was commercial alumina (flexicord PURE ALUMINA 99.7, Saint-Gobain, Avignon, France) with a feed rate of 0.3 m/min. The time of spraying was approximately 25 s per pin, the spraying distance was ≈ 150 mm between the flame spraying gun and the substrate material and the estimated flame temperature was 3080–3160 °C. After cooling, the specimens were removed from the graphite substrate and milled for 60 s at 800 rpm using a vibratory disc mill MSL2 (VEB BHKE, Freiberg, Germany) with steel-made grinding tools.

2.2. Sample Characterisation and Heat Treatment

The material was studied using X-ray powder diffraction (XRD) (Empyrean, Malvern Panalytical GmbH, Kassel, Germany) in combination with Rietveld refinement using HighScore Plus 4.8 (Malvern Panalytical B.V., Almelo, The Netherlands). XRD measurements were taken using Cu-K α_1 radiation between 10 and 140° 2 Θ with a 0.0143° step size and an exposure of 160 s/step in Bragg–Brentano geometry, which resulted in an overall measurement time of roughly 53 min. On the incident side, a divergence slit of 1/8° and an anti-scatter slit of 1/2° were applied, together with 0.04 rad soller slits on the incident and detector sides.

Thermal treatment of the samples was performed in situ using a high-temperature XRD chamber (HTK 1200N, Anton-Paar GmbH, Graz, Austria) with a dense-sintered alumina sample holder, which was used for measurements in the temperature range between room temperature and 1200 °C. For that, the zero-point height and the ω -offset of the sample was determined before the measurement by using a parallel beam setup.

The as-sprayed material was investigated using two approaches. The thermal expansion and phase transitions were studied by heating the material in steps of 25 K up to the highest temperature. After each heating step, the system was rested for 5 min before the XRD measurements started.

In subsequent experiments, the as-sprayed material was held isothermally at 1000 °C and 1100 °C (samples T-1000 and T-1100, respectively) for a time of 30 h to study the structural changes with time at a constant temperature. XRD measurements were taken after each hour and after two hours between 1 and 10 h and 10 and 30 h of heat treatment, respectively. To prevent further structural changes during the measurement at the annealing temperature, the samples were cooled down for XRD measurements to a temperature of 600 °C, at which no substantial reordering was detected and the high-temperature state could be assumed to be quenched. After XRD measurements, the sample was heated again to the respective annealing temperature. The applied heating and cooling rate was always

10 K/min. It should be mentioned that the sample holder was not actively cooled, but the outer walls of the heating chamber were. As a consequence, the achievable cooling rates decrease with a decrease in temperature. However, it was observed that the nominal cooling rate was achieved with only small deviations in the temperature range between 1200 °C and 600 °C.

Next, the thermal expansion of these isothermally heat-treated powders were investigated in the same way as the as-sprayed material before.

2.3. Thermal Expansion Coefficient

The obtained volumes of the elemental cells for the phases α -, η -, δ_1 - and θ -Al₂O₃ with temperature $V(T)$ were used to determine the volumetric thermal expansion coefficient α_V as follows. A set of five consecutive datapoints were fitted by $V(T) = a + b \cdot T + c \cdot T^2$ and its derivative was then used to calculate α_V for each 3rd point according to

$$\alpha_V = \frac{1}{V} \cdot \frac{\partial V}{\partial T}. \quad (1)$$

It should be mentioned that for the first two and the last two investigated temperatures, the thermal expansion coefficients were calculated using the derived parameters of the first and last least-square fit of the whole dataset, respectively. Using such an approach to derive α_V from the experimental data instead of fitting one equation for all data points results in a scattered $\alpha_V(T)$ curve but reproduces the observed overall changes in volume with a higher accuracy in comparison to the one-equation method.

3. Results

Typical XRD patterns are presented as an example in Figures 1 and 2 for the as-sprayed material obtained at the temperatures of 1000 °C and 1200 °C, respectively. The obtained reflections were indexed using the structure models of α -Al₂O₃ (#ICSD-73725 [33]), η -Al₂O₃ (#ICSD-39104 [20]), δ_1 -Al₂O₃ [25] and θ -Al₂O₃ (#ICSD-82504 [34]). No other δ -variants were detected in the analysed diffraction pattern. It should be noted that the structure model for η -Al₂O₃ was taken in favour of γ -Al₂O₃ (#ICSD-95302 [35]) as the agreement between the calculated and observed intensities were much better with the cubic η -model. It might be the case that flame- or plasma-sprayed aluminas form the η -variant instead of the defect spinel type.

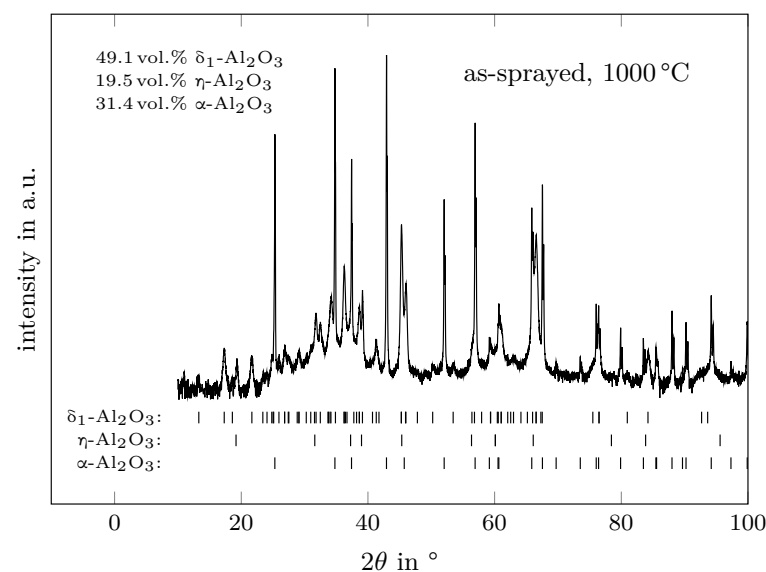


Figure 1. Determined XRD pattern of the as-sprayed material at 1000 °C showing the reflections of η -, δ_1 - and α -Al₂O₃.

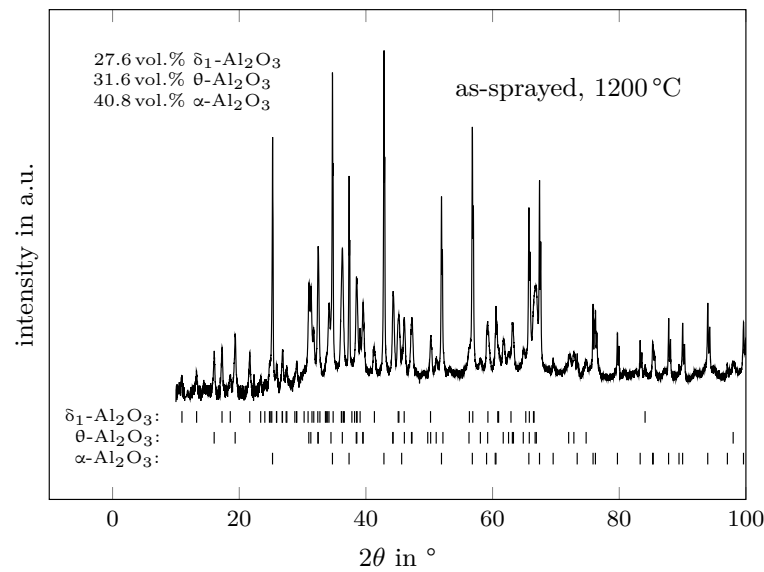


Figure 2. Determined XRD pattern of the as-sprayed material at 1200 °C showing the reflections of θ -, δ_1 - and α - Al_2O_3 .

3.1. Phase Transformations of the Flame-Sprayed Sample

The as-sprayed sample consisted of 30 vol.% α - Al_2O_3 and δ_1 - Al_2O_3 , respectively, and 40 vol.% η - Al_2O_3 . With heating up to 900 °C, approximately 8 vol.% of η - Al_2O_3 transformed into the δ_1 polymorph. In the temperature range above 900 °C, until it completely vanished between 1100 °C and 1025 °C, η - Al_2O_3 was mostly transformed into δ_1 - Al_2O_3 with an increased transition rate. After reaching a maximum of 55 vol.% at 1025–1050 °C, the amount of δ_1 decreased to 28 vol.% at 1200 °C. θ - Al_2O_3 was formed at temperatures higher than 1025 °C and its amount increased constantly up to 32 vol.% at 1200 °C. One can say that all observed transformation rates occurred linearly with temperature, only the amount of α - Al_2O_3 increased nonlinearly at temperatures above 950 °C, as it can be deduced from Figure 3. The transition rates of η -, δ_1 - and θ - Al_2O_3 , which were obtained by least-square fitting, are summarised in Table 1.

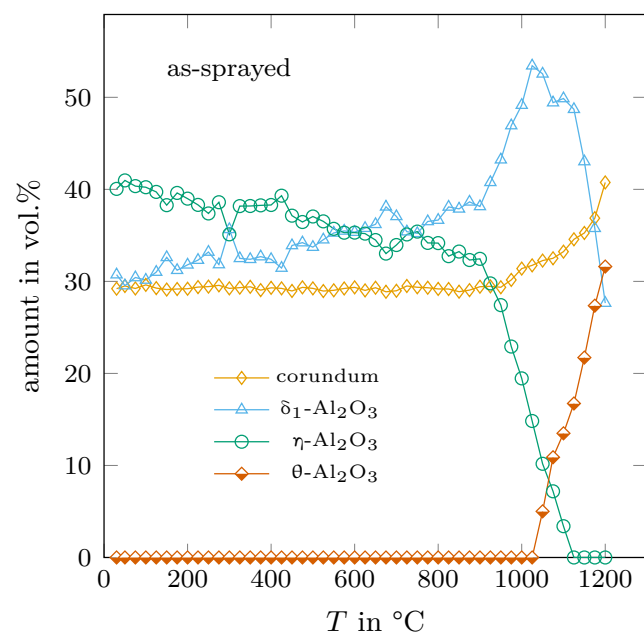


Figure 3. Determined trend of the phase composition with temperature of the as-sprayed sample.

Table 1. Determined transition rates of the metastable aluminas from the as-sprayed sample.

Phase	Temperature Range: Transition Rate in vol.%/K		
η -Al ₂ O ₃	30–900 °C: −0.0089	900–1125 °C: −0.1505	
δ_1 -Al ₂ O ₃	30–900 °C: 0.0091	900–1025 °C: 0.1204	1125–1200 °C: −0.2817
θ -Al ₂ O ₃	1025–1200 °C: 0.1756		

Two things are remarkable here: (1) The linear transition rates show that the transformation sequence $\eta \rightarrow \delta_1 \rightarrow \theta + \alpha$ is not limited by kinetic effects (even close to room temperature). If it was so, the transition rates should increase with increasing temperature. (2) The measurements confirmed that the densities of the observed aluminas are different and show the general sequence $\rho(\theta) < \rho(\eta) < \rho(\delta_1) < \rho(\alpha)$. It is interesting that after the formation of the relatively dense δ_1 phase, it is partially transformed into the least dense θ -Al₂O₃. Therefore, the transformation path of the metastable aluminas to the thermodynamically stable α -variant does not follow the simple assumption that the lattices are transformed step by step in the direction of the stablest structure, e.g., from a low-density variant to the densest α -Al₂O₃ phase.

In the following, a model will be presented that is able to explain the experimental findings and that gives proposes the driving force for the transitions of the metastable aluminas. As the transformations seem not to be thermally activated, another process must be in charge that induces a constant phase transition even at low temperatures. Thermal expansion could be a candidate, and it was found that slight differences in the thermal expansion of the phases in question are key to understanding the observations. In Figure 4a, the ratios of the measured cell volumes (per formula unit of Al₂O₃) of η : α and η : δ_1 are shown. Up to a temperature of 800 °C, η and δ_1 show the same thermal expansion, but the thermal expansion coefficient of α -Al₂O₃ is larger than the one of η , resulting in a constantly decrease in the corresponding volume ratio. With 40 vol.% η -Al₂O₃ in the as-sprayed state, it can be assumed that α -Al₂O₃ was dispersed and formed a nucleus in the η -Al₂O₃ matrix. With a larger thermal expansion coefficient, the α -Al₂O₃ grains will induce pressure on the surrounding matrix on heating. This stress can be reduced by crack formation or phase transformation. In the latter case, the transition from η - to δ_1 -Al₂O₃ is promising as the density of δ_1 is larger than that of η , which means that an open volume can be created during transition that can be filled by α -Al₂O₃ with increasing temperature.

With a derived dataset indexed with i , the fraction of the created free volume per transformed volume of η -Al₂O₃, f_{open} , can be calculated by

$$f_{\text{open}} = 1 - f_{\eta \rightarrow \delta_1} = 1 - \frac{V_i^{\delta_1}}{V_{i-1}^{\eta}}, \quad (2)$$

where V_i^* and V_{i-1}^* are the respective cell volumes at the current temperature T_i and at the preceding one at T_{i-1} , respectively, with $*$ \in $\{\delta_1, \eta, \alpha\}$. The amount of transformed η -Al₂O₃ is then given by

$$\Delta n_V^{\eta \rightarrow \delta_1} = f_{\text{open}} \cdot n_V^{\eta} \cdot f^{\eta}, \quad (3)$$

where f^{η} is the fraction of the amount of η , n_V^{η} , that is transformed on heating. In a similar way, the necessary volume for α -Al₂O₃ can be calculated from the change in the V^{η}/V^{α} ratio. The volume ratios were fitted with

$$r^*(T) = a + b \cdot T + c \cdot \exp(T - 600)^d \quad (4)$$

as it can be seen in Figure 4a. The change in the ratio is then simply calculated with $\Delta r^\alpha = r^\alpha(T_i) - r^\alpha(T_{i-1})$ using $a = 1.0934$, $b = -2.68407 \cdot 10^{-6}/^\circ\text{C}$, $c = 1.7055 \cdot 10^{-5}$ and $d = 0.0139101$. The additional volume for α is then

$$\Delta n_V^\alpha = \Delta r_i^\alpha \cdot n_{V,i}^\alpha. \quad (5)$$

With that, the transition rate of the volume of the η - Al_2O_3 can be calculated by

$$\frac{\Delta n_V^\eta}{\Delta T} = \frac{\Delta n_V^\alpha \cdot n_V^\eta}{\Delta n_V^{\eta \rightarrow \delta_1} \cdot \Delta T} = \frac{\Delta r_i^\alpha \cdot n_{V,i}^\alpha}{f_{\text{open}} \cdot \Delta T}. \quad (6)$$

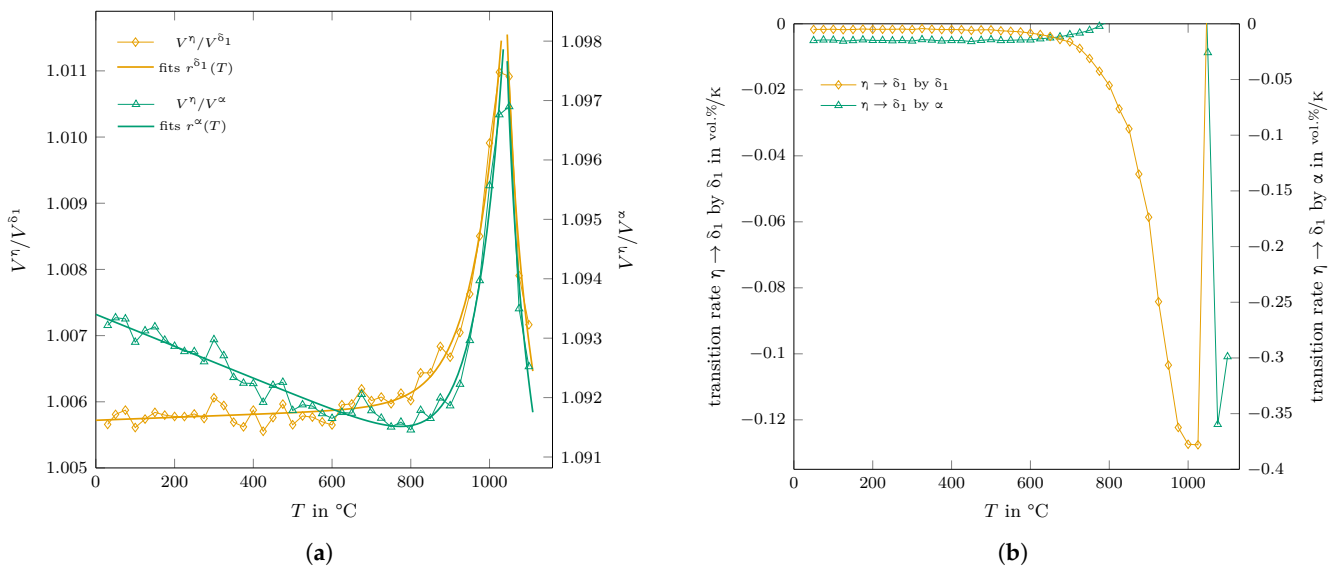


Figure 4. Calculated (a) ratios of the cell volumes (per formula unit of Al_2O_3) for η - Al_2O_3 : δ_1 - Al_2O_3 and η - Al_2O_3 : α - Al_2O_3 and (b) maximum transition rate of the $\eta \rightarrow \delta_1$ reaction induced by the thermal expansion of δ_1 - and α - Al_2O_3 .

The calculated maximum transition rate for this reaction is shown in Figure 4b. The calculated rate has a maximum value of $-0.13 \text{ vol.}\%/K$ at around $1000 \text{ }^\circ\text{C}$, relatively close to the experimentally determined one of $-0.09 \text{ vol.}\%/K$ (see Table 1), which means that approximately a maximum of 69% of the possible η volume is affected by the induced stress field of the α expansion.

For temperatures above $600 \text{ }^\circ\text{C}$, the thermal expansion of η - Al_2O_3 becomes increasingly larger than those of the δ_1 and α phases, showing the largest volume ratios between 1025 and $1050 \text{ }^\circ\text{C}$. The induced pressure on the η lattice by α - Al_2O_3 and the resulting transition rate disappeared just below $800 \text{ }^\circ\text{C}$, as can be seen in Figure 4b. With a reducing volume amount of η , δ_1 - Al_2O_3 became the dominant phase in the phase assemblage of the investigated sample from $600 \text{ }^\circ\text{C}$ up to $1100 \text{ }^\circ\text{C}$. Upon losing its matrix character, η - Al_2O_3 induces pressure within the formed δ_1 matrix due to the differences in thermal expansion. Consequently, the transition rate for the second induced $\eta \rightarrow \delta_1$ transition can be estimated as

$$\frac{\Delta n_{V,i}^\eta}{\Delta T} = \frac{\Delta r_i^{\delta_1} \cdot n_{V,i-1}^\eta}{f_{\text{open}} \cdot \Delta T}, \quad (7)$$

using $a = 1.00572$, $b = 2.23484 \cdot 10^{-7}/^\circ\text{C}$, $c = 1.54154 \cdot 10^{-5}$ and $d = 0.0136704$ for $r^{\delta_1}(T)$. For this reaction, a transition rate of $\approx -0.002 \text{ vol.}\%/K$ was found up to a temperature of $550 \text{ }^\circ\text{C}$, which increased up to $-0.128 \text{ vol.}\%/K$ at $1025 \text{ }^\circ\text{C}$ (see Figure 4b). The transition rates obtained from the Rietveld refinement (Table 1) were $0.12 \text{ vol.}\%/K$ for δ_1 formation and $-0.15 \text{ vol.}\%/K$ for the η decomposition above $900 \text{ }^\circ\text{C}$.

3.2. Structural Changes in δ_1 -Al₂O₃ and η -Al₂O₃

The δ_1 phase undergoes a structural change under heating independent of the heat treatment history, as shown in Figure 5. Its lattice parameters show an anisotropic thermal expansion. After reaching a maximum value (at ≈ 950 °C for the as-sprayed sample and at ≈ 1100 °C and 1175 °C for the T-1000 and T-1100 samples, respectively), the lattice parameter b decreases on heating up to the maximum temperature of 1200 °C, whereas the length of the c -axis significantly increases at temperatures above 900 °C. It seems that for both axes, the lattice parameters of the as-sprayed and the annealed δ_1 phases tend to (or would tend if stable enough) to reach the same value at 1200 °C and above, respectively. In comparison, the values of the lattice parameter a were almost the same in as-cast and the T-1000 state and the T-1100 values were found to be slightly lower. In general, the a values increase with temperature with a pronounced hump for the as-cast state and a maximum at around 1050 °C. This effect is less dramatic in case of the T-1000 sample and was not detected for the T-1100 sample. The respective extension of the overall structural changes in δ_1 -Al₂O₃ were the largest for the as-sprayed state and decreased with increasing annealing temperature.

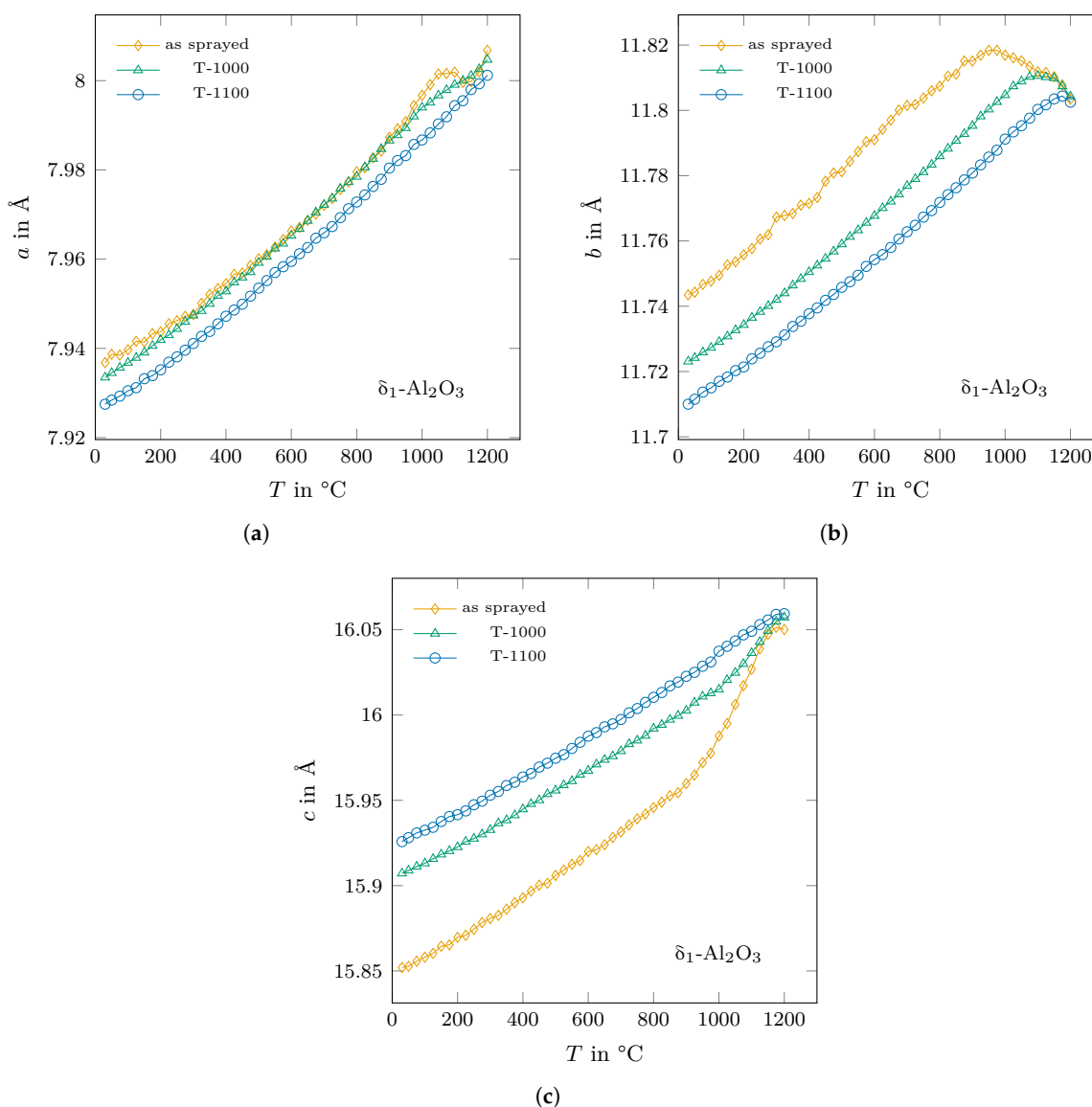


Figure 5. The trend of the lattice parameters (a–c) of δ_1 -Al₂O₃ with temperature for the as-sprayed sample and for the ones annealed at 1000 °C and 1100 °C, respectively.

Similarly, a strong increase in the volume of the cubic η - Al_2O_3 was observed at temperatures above 900 °C until it was fully transformed at ≈ 1050 °C.

3.3. Structural Changes at a Constant Temperature

The phase relations among the different alumina structures were studied using annealing experiments at 1000 °C and 1100 °C. Especially for the δ_1 - Al_2O_3 variant, distinct structural changes were observed, for example, the lattice dimension in a - and b -direction decreased whereas that in the c -direction strongly increased with time. However, the volume of the unit cell stayed almost constant after five hours annealing at 1000 °C, whereas the unit cell volume decreased almost constantly during annealing at 1100 °C. Interestingly, the cell volumes in both experiments were always above the value that was obtained during the thermal expansion measurement of the as-sprayed sample (heated in steps of 25 K followed by a roughly one hour holding time), as can be seen in Figure 6.

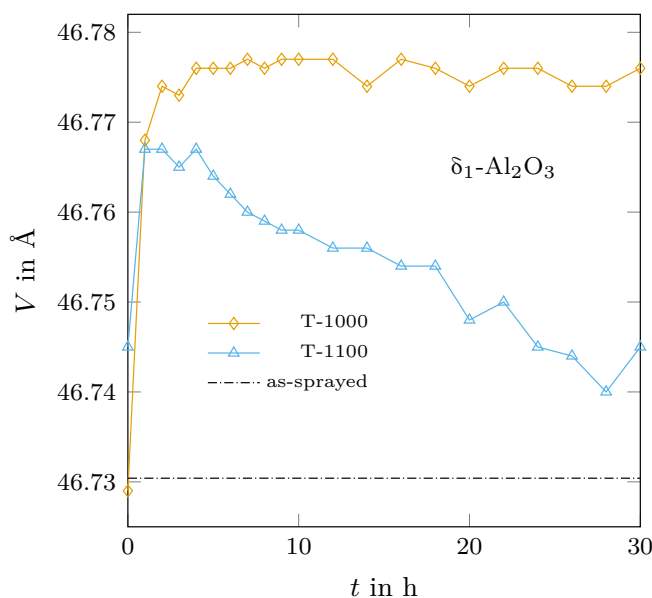


Figure 6. Determined molar volumes of δ_1 - Al_2O_3 measured at 600 °C for the isothermally held samples in comparison to the value of the as-sprayed material obtained during the thermal expansion experiment.

Even the δ_1 -variant showed the strongest structural changes with annealing time, there were changes in all phases—even some slight ones in α - Al_2O_3 . It can be assumed that a change in lattice dimensions modifies the surface energy of the crystals, which could be a driving force for further phase transitions as well. Figure 7 shows the determined trend of the phase assemblages of the two experiments. η - Al_2O_3 transformed mainly into δ_1 during annealing at 1000 °C but also the contents of α - and θ - Al_2O_3 increased. The latter was not detected until 1050 °C in the case of 25 K-step heating of the as-sprayed material. In comparison, at 1100 °C, δ_1 - Al_2O_3 transformed into θ - and α - Al_2O_3 in agreement with the findings of Wilson and McConnell [16].

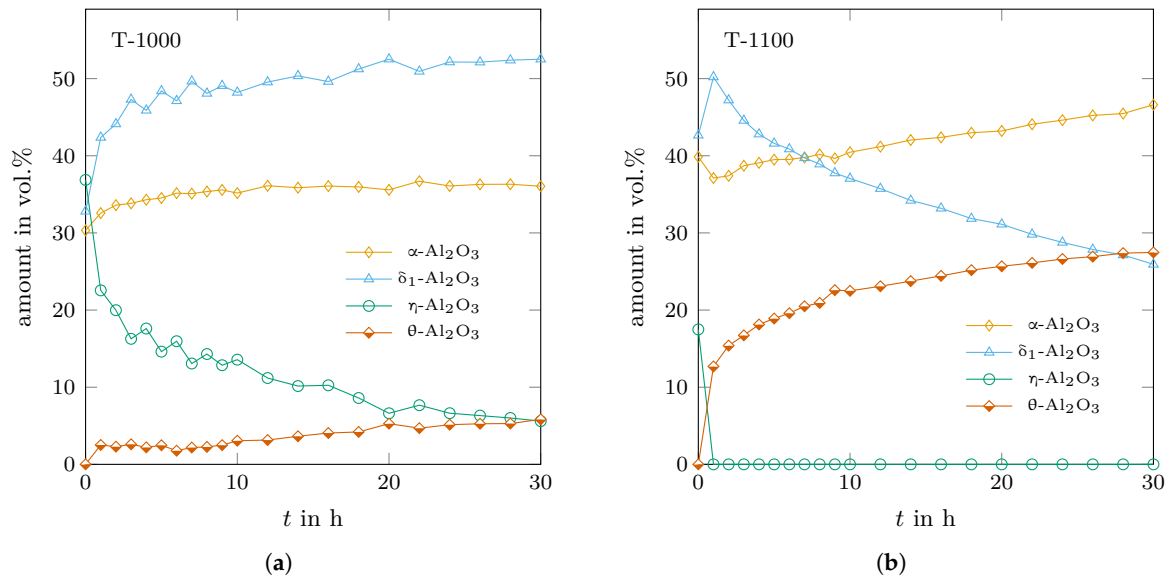


Figure 7. Determined trends of the phase assemblages with time for the samples annealed at (a) 1000 °C and (b) 1100 °C.

3.4. Thermal Expansion of Corundum and the Transition Aluminas

The thermal expansion of α-Al₂O₃ was determined as a reference to validate the chosen method for determining the thermal expansion coefficient. The determined cell volume and the corresponding calculated thermal expansion coefficient are shown in comparison with reported data from the literature in Figure 8. For the latter, the calculated values closely follow the reference data [36] up to temperatures of approximately 950 °C. Above, the thermal expansion coefficient of all three samples shows a slight minimum of ≈10% below the reference value at around 1050 °C after it increases up to the reference value at 1200 °C.

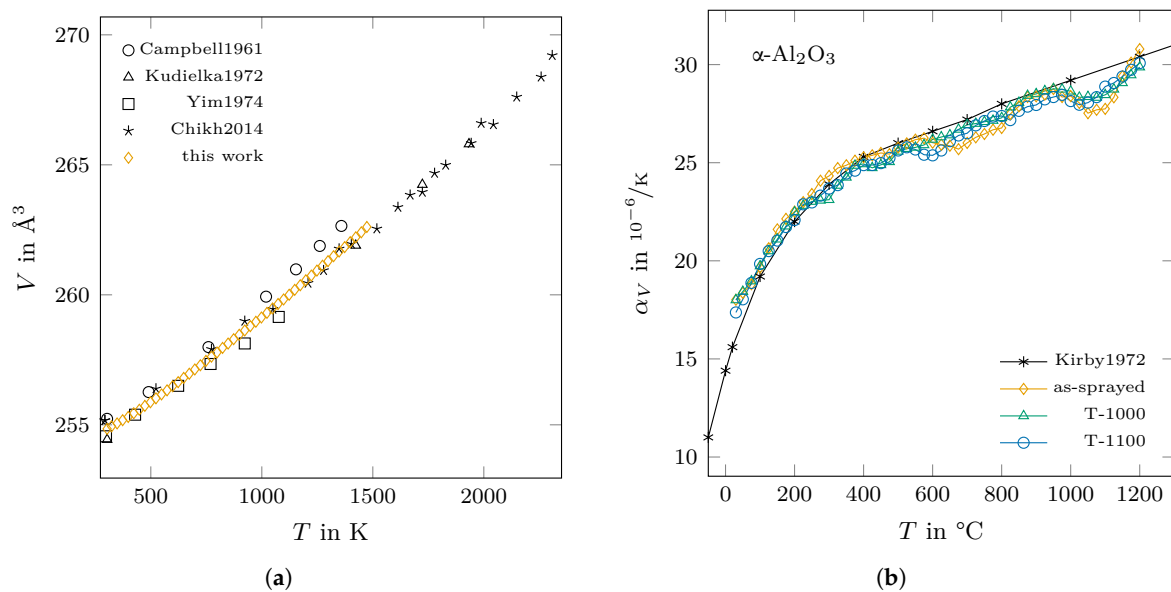


Figure 8. Thermal expansion of α-Al₂O₃: (a) determined volumes of the elemental cell in comparison to the literature (Campbell and Grain (1961) [37], Kudielka (1972) [38], Yim and Paff (1974) [39] and Chikh et al. (2014) [40]) and (b) the derived thermal expansion coefficients of the as-sprayed and annealed samples in comparison to reference data from Kirby et al. (1972) [36].

Overall, the used method of determining the thermal expansion coefficient from the measured volume values worked within an acceptable range of scatter. Therefore, it was also applied to analyse the data of the transition aluminas.

As it can be expected from the presented lattice parameters in Figure 5, the thermal expansion coefficient of δ_1 -Al₂O₃ differs much between the as-sprayed and the annealed states in the temperature range between 850 °C and 1100 °C, as can be seen in Figure 9a. For the annealed δ_1 phase, the values of α_V range from $16.5 \cdot 10^{-6}/\text{K}$ at room temperature to $25.2 \cdot 10^{-6}/\text{K}$ at 1000 °C before they drop to $5.1 \cdot 10^{-6}/\text{K}$ at a temperature of 1200 °C. In comparison, the as-sprayed state shows a similar trend of α_V up to a temperature of 850 °C, then strongly increases up to a value of $31.5 \cdot 10^{-6}/\text{K}$ at 1000 °C and finally decreases in value in the same way as the annealed phases.

The determined trend of the thermal expansion coefficient of the as-sprayed η -Al₂O₃ showed a similar behaviour as the as-sprayed δ_1 phase (see Figure 9b). Here, α_V ranged from $17.6 \cdot 10^{-6}/\text{K}$ at room temperature to $32.4 \cdot 10^{-6}/\text{K}$ at 875 °C, before it reached a maximum value of $71.1 \cdot 10^{-6}/\text{K}$ at 975 °C and dropped below zero for temperatures above 1025 °C.

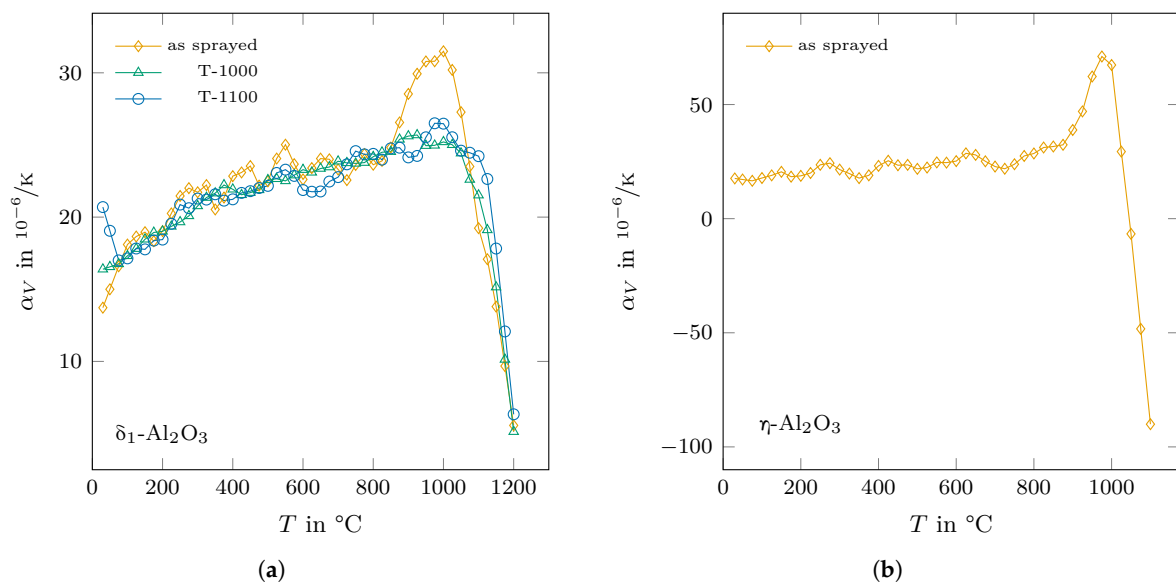


Figure 9. Determined thermal expansion coefficients of (a) for δ_1 -Al₂O₃ for the as-sprayed and the annealed states and (b) for the as-sprayed η -Al₂O₃.

4. Discussion

The transformation of the metastable aluminas to the final α -Al₂O₃ formation is a complex interplay between structural changes, surface energy and crystal defects. Based on the results of this work, it is suggested that the η (γ) \rightarrow δ_1 \rightarrow θ transformation sequence is, at least in parts, mechanically induced. Such transformations of boehmite-derived metastable aluminas to α -Al₂O₃ were reported, e.g., in [41–44], to be triggered by milling processes. As already shown by Wilson and McConnel [16], the transformation sequence is also a question of time at constant temperatures. In the current work, it was shown that the phases undergo some structural changes as well, which can be related to a rearrangement of the atoms within the unit cell. Such internal ordering influences properties such as the surface energy and can thus influence the thermodynamic-based relations of the different crystals at their interfaces, inducing further transformations.

After a 30 h annealing time, the T-1000 and T-1100 samples were heated and characterised by XRD in the same procedure as the as-sprayed sample. Figure 10 shows the obtained δ_1 -Al₂O₃ content for the three samples. The annealed samples showed no change in their phase contents up to the respective annealing temperatures. Above these temperatures, the amounts of δ_1 -Al₂O₃ were then dramatically reduced up to 1200 °C. It is worth

noting that in case of the as-sprayed and the T-1000 sample, the thermal history seems to have only a slight influence on the phase content and the kinetics of the δ_1 decomposition above 1000 °C, whereas the lattice dimensions were quite different at the same time (see Figure 5).

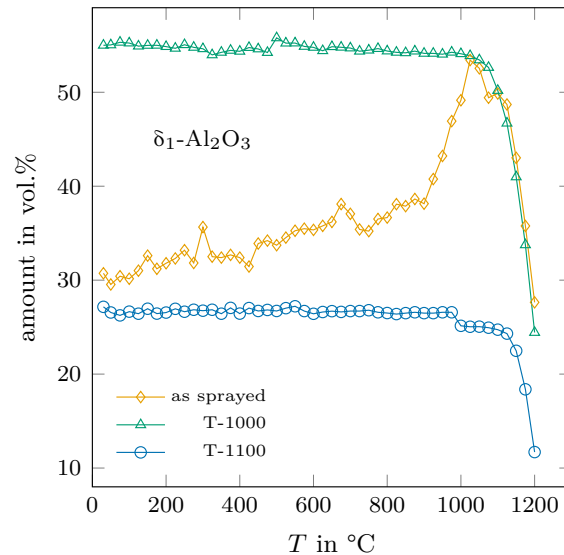


Figure 10. Determined amounts of δ_1 - Al_2O_3 for the as-sprayed sample and for the ones annealed at 1000 °C and 1100 °C, respectively.

A direct $\gamma \rightarrow \theta$ transition was reported in [1] and such a transition seems to also be indicated in the presented work. The determined trends of density for the transition aluminas of the as-sprayed sample with temperature are shown in Figure 11. As already mentioned in Section 3.2, the volume of the elemental cell of η - Al_2O_3 strongly increases above 900 °C, leading to a corresponding decrease in density. The density values of η - and θ - Al_2O_3 are seamlessly connected between the temperatures of 1050 °C and 1075 °C. Such behaviour would indicate a second-order phase transition. The two density values above 1050 °C for η - Al_2O_3 and the one at 1050 °C for θ - Al_2O_3 are ignored here. The respective phase contents were already below 5%, and with no presence of distinct (and strong) reflections in the diffraction pattern, the uncertainty of the determined lattice parameters might be too large for a correct determination.

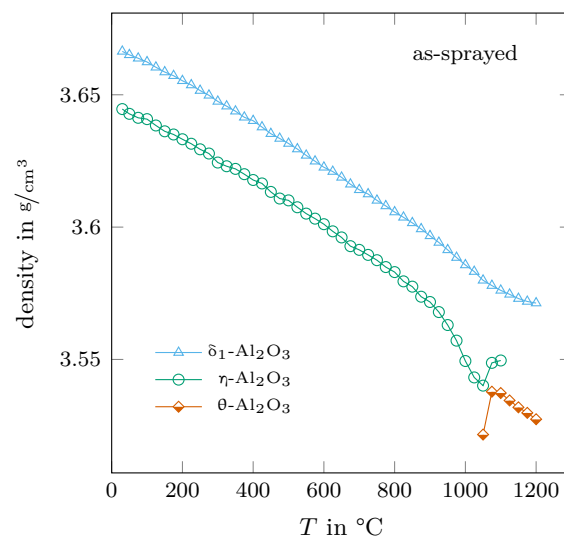


Figure 11. Determined densities of the metastable aluminas present in the as-sprayed sample.

From a technological point of view, the large values of thermal expansion on first heating observed for η -Al₂O₃ and δ ₁-Al₂O₃ can be problematic in the fast heating of such coatings. At the least, crack propagation can be expected or—even worse—spalling effects might occur. One should also keep in mind that the flame-sprayed material is relatively dense perpendicular to the surface but shows extensive pore networks along the surface due to its two-dimensional layered character on the macroscale. The available pore dimensions will also influence the extension of pressure-induced phase transitions, which must be taken into account when interpreting the results of this work as micropores could still be present after milling the flame-sprayed coating.

Supplementary Materials: The following are available online at <https://www.mdpi.com/article/10.3390/cryst13050743/s1>.

Author Contributions: Conceptualization, T.Z.; data curation, T.Z.; formal analysis, T.Z.; methodology, T.Z.; validation, T.Z.; investigation, T.Z.; resources C.G.A.; writing—original draft preparation, T.Z.; writing—review and editing, T.Z. and C.G.A.; visualization, T.Z.; project administration, C.G.A.; funding acquisition, C.G.A. All authors have read and agreed to the published version of the manuscript.

Funding: This research was funded by the German Research Foundation (DFG) within the Research Unit FOR 3010 (project number: 416817512). The X-ray diffractometer was acquired through the “Major Research Instrumentation” funding programme of the German Research Foundation (DFG), reference number: INST 267/157-1 FUGG (project number: 395259190).

Data Availability Statement: The data presented in this study are available on request from the corresponding author. The main results of the Rietveld analysis and the processed thermal expansion data can be found in the Supplementary Files.

Acknowledgments: We are grateful for the sample preparation by Florian Kerber.

Conflicts of Interest: The authors declare no conflict of interest. The funders had no role in the design of the study; in the collection, analyses, or interpretation of data; in the writing of the manuscript; or in the decision to publish the results.

References

1. Lee, J.; Jeon, H.; Oh, D.G.; Szanyi, J.; Kwak, J.H. Morphology-dependent phase transformation of γ -Al₂O₃. *Appl. Catal. A Gen.* **2015**, *500*, 58–68. [CrossRef]
2. Kovarik, L.; Bowden, M.; Szanyi, J. High temperature transition aluminas in δ -Al₂O₃/ θ -Al₂O₃ stability range: Review. *J. Catal.* **2021**, *393*, 357–368. [CrossRef]
3. Dager, A.; Fargeot, D. T.E.M. study of Al₂O₃ metastable phases. *Radiat. Eff.* **1983**, *74*, 279–289.
4. Nordahl, C.S.; Messing, G.L. Thermal analysis of phase transformation kinetics in α -Al₂O₃ seeded boehmite and γ -Al₂O₃. *Thermochim. Acta* **1998**, *318*, 187–199. [CrossRef]
5. Fargeot, D.; Mercurio, D.; Dager, A. Structural characterization of alumina metastable phases in plasma sprayed deposits. *Mater. Chem. Phys.* **1990**, *24*, 299–314. [CrossRef]
6. Damani, R.; Makroczy, P. Heat treatment induced phase and microstructural development in bulk plasma sprayed alumina. *J. Eur. Ceram. Soc.* **2000**, *20*, 867–888. [CrossRef]
7. Di Girolamo, G.; Brentari, A.; Blasi, C.; Serra, E. Microstructure and mechanical properties of plasma sprayed alumina-based coatings. *Ceram. Int.* **2014**, *40*, 12861–12867. [CrossRef]
8. Rudolph, M.; Motylenko, M.; Rafaja, D. Structure model of γ -Al₂O₃ based on planar defects. *IUCr* **2019**, *6*, 116–127. [CrossRef]
9. Levin, I.; Brandon, D. Metastable Alumina Polymorphs: Crystal Structures and Transition Sequences. *J. Am. Ceram. Soc.* **1998**, *81*, 1995–2012. [CrossRef]
10. Paglia, G.; Božin, E.S.; Billinge, S.J. Fine-Scale Nanostructure in γ -Al₂O₃. *Chem. Mater.* **2006**, *18*, 3242–3248.
11. Pardo, P.; Alarcón, J. Thermal stability of transition alumina nanocrystals with different microstructures. *Ceram. Int.* **2018**, *44*, 11486–11496. [CrossRef]
12. Deng, L.; Han, S.; Zhou, D.; Li, Y.; Shen, W. Morphology dependent effect of γ -Al₂O₃ for ethanol dehydration: Nanorods and nanosheets. *CrystEngComm* **2022**, *24*, 796–804. [CrossRef]
13. Feng, H.; Wang, H.; Ma, Z.; Wang, S.; Li, P. Quantification of surface orientation effect on the thermal stability of γ -Al₂O₃ with different morphologies. *Appl. Surf. Sci.* **2022**, *594*, 153509. [CrossRef]

14. Bolelli, G.; Cannillo, V.; Gadow, R.; Killinger, A.; Lusvardi, L.; Manfredini, T.; Müller, P. Properties of Al₂O₃ coatings by High Velocity Suspension Flame Spraying (HVSFS): Effects of injection systems and torch design. *Surf. Coat. Technol.* **2015**, *270*, 175–189. [[CrossRef](#)]
15. Rudolph, M.; Salomon, A.; Schmidt, A.; Motylenko, M.; Zienert, T.; Stöcker, H.; Himcinschi, C.; Amirkhanyan, L.; Kortus, J.; Aneziris, C.G.; et al. Thermally Induced Formation of Transition Aluminas from Boehmite. *Adv. Eng. Mater.* **2017**, *19*, 1700141. [[CrossRef](#)]
16. Wilson, S.; Mc Connell, J. A kinetic study of the system γ -AlOOH/Al₂O₃. *J. Solid State Chem.* **1980**, *34*, 315–322. [[CrossRef](#)]
17. Kovarik, L.; Bowden, M.; Shi, D.; Washton, N.M.; Andersen, A.; Hu, J.Z.; Lee, J.; Szanyi, J.; Kwak, J.h.; Peden, C.H. Unraveling the Origin of Structural Disorder in High Temperature Transition Al₂O₃: Structure of θ -Al₂O₃. *Chem. Mater.* **2015**, *27*, 7042–7049. [[CrossRef](#)]
18. Pecharrmán, C.; Sobrados, I.; Iglesias, J.; González-Carreño, T.; Sanz, J. Thermal Evolution of Transitional Aluminas Followed by NMR and IR Spectroscopies. *J. Phys. Chem. B* **1999**, *103*, 6160–6170.
19. Xu, S.; Jaegers, N.R.; Hu, W.; Kwak, J.H.; Bao, X.; Sun, J.; Wang, Y.; Hu, J.Z. High-Field One-Dimensional and Two-Dimensional ²⁷Al Magic-Angle Spinning Nuclear Magnetic Resonance Study of θ -, δ -, and γ -Al₂O₃ Dominated Aluminum Oxides: Toward Understanding the Al Sites in γ -Al₂O₃. *ACS Omega* **2021**, *6*, 4090–4099.
20. Shirasuka, K.; Yanagida, H.; Yamaguchi, G. The Preparation of η Alumina and its Structure. *J. Ceram. Assoc.* **1976**, *84*, 610–613. [[CrossRef](#)]
21. Paglia, G.; Rohl, A.L.; Buckley, C.E.; Gale, J.D. Determination of the structure of γ -alumina from interatomic potential and first-principles calculations: The requirement of significant numbers of nonspinel positions to achieve an accurate structural model. *Phys. Rev. B* **2005**, *71*, 224115. [[CrossRef](#)]
22. Samain, L.; Jaworski, A.; Edén, M.; Ladd, D.M.; Seo, D.K.; Javier Garcia-Garcia, F.; Häussermann, U. Structural analysis of highly porous γ -Al₂O₃. *J. Solid State Chem.* **2014**, *217*, 1–8. [[CrossRef](#)]
23. Paglia, G.; Buckley, C.E.; Rohl, A.L.; Hart, R.D.; Winter, K.; Studer, A.J.; Hunter, B.A.; Hanna, J.V. Boehmite Derived γ -Alumina System. 1. Structural Evolution with Temperature, with the Identification and Structural Determination of a New Transition Phase, γ' -Alumina. *Chem. Mater.* **2004**, *16*, 220–236.
24. Luo, Z. Structure of boehmite-derived γ -alumina and its transformation mechanism revealed by electron crystallography. *Acta Crystallogr. Sect. B* **2021**, *77*, 772–784. [[CrossRef](#)]
25. Kovarik, L.; Bowden, M.; Genc, A.; Szanyi, J.; Peden, C.H.; Kwak, J.H. Structure of δ -Alumina: Toward the Atomic Level Understanding of Transition Alumina Phases. *J. Phys. Chem. C* **2014**, *118*, 18051–18058. [[CrossRef](#)]
26. Kovarik, L.; Bowden, M.; Shi, D.; Szanyi, J.; Peden, C.H. Structural Intergrowth in θ -Al₂O₃. *J. Phys. Chem. C* **2019**, *123*, 9454–9460. [[CrossRef](#)]
27. Kovarik, L.; Bowden, M.; Andersen, A.; Jaegers, N.R.; Washton, N.; Szanyi, J. Quantification of High-Temperature Transition Al₂O₃ and Their Phase Transformations. *Angew. Chem. Int. Ed.* **2020**, *59*, 21719–21727.
28. Zienert, T.; Endler, D.; Hubálková, J.; Eusterholz, M.; Boll, T.; Heilmaier, M.; Günay, G.; Weidner, A.; Biermann, H.; Kraft, B.; et al. Coarse-grained refractory composite castables based on alumina and niobium. *Adv. Eng. Mater.* **2022**, *24*, 2200296. [[CrossRef](#)]
29. Günay, G.; Zienert, T.; Endler, D.; Aneziris, C.G.; Biermann, H.; Weidner, A. High-temperature compressive behavior of refractory alumina-niobium composite material. *Adv. Eng. Mater.* **2022**, *24*, 2200292. [[CrossRef](#)]
30. Kraft, B.; Wagner, S.; Hoffmann, M.J. Field Assisted Sintering of Nb-Al₂O₃ Composite Materials and Investigation of Electrical Conductivity. *Adv. Eng. Mater.* **2022**, *24*, 202200063. [[CrossRef](#)]
31. Zienert, T.; Farhani, M.; Dudczig, S.; Aneziris, C.G. Coarse-grained refractory composites based on Nb-Al₂O₃ and Ta-Al₂O₃ castables. *Ceram. Int.* **2018**, *44*, 16809–16818. [[CrossRef](#)]
32. Aneziris, C.G.; Gehre, P.; Kratschmer, T.; Berek, H. Thermal Shock Behavior of Flame-Sprayed Free-Standing Coatings Based on Al₂O₃ with TiO₂- and ZrO₂-Additions. *Int. J. Appl. Ceram. Technol.* **2011**, *8*, 953–964.
33. Maslen, E.; Streltsov, V.; Streltsova, N.; Ishizawa, N.; Satow, Y. Synchrotron X-ray study of the electron density in α -Al₂O₃. *Acta Crystallogr. Sect. B* **1993**, *49*, 973–980. [[CrossRef](#)]
34. Husson, E. Structural studies of transition aluminas. Theta alumina. *Eur. J. Solid State Inorg. Chem.* **1996**, *33*, 1223–1231.
35. Gutiérrez, G.; Taga, A.; Johansson, B. Theoretical structure determination of γ -Al₂O₃. *Phys. Rev. B* **2001**, *65*, 012101. [[CrossRef](#)]
36. Kirby, R.K.; Hahn, T.A.; Rothrock, B.D. *American Institute of Physics Handbook—4f: Thermal Expansion*, 3rd ed.; McGraw-Hill Book Company: New York, NY, USA, 1972.
37. Campbell, W.J.; Grain, C. Thermal Expansion of Alpha-Alumina. *Adv. X-ray Anal.* **1961**, *5*, 244–256. [[CrossRef](#)]
38. Kudielka, H. Die thermische Ausdehnung der isotypen Mischreihen-Endglieder Cr₂O₃ und α -Al₂O₃, ermittelt mit einer neuen, lichtstarken Seemann-Bohlin-Kammer. *Monatshfte Chem.* **1972**, *103*, 72–80. [[CrossRef](#)]
39. Yin, W.; Paff, R. Thermal expansion of AlN, sapphire, and silicon. *J. Appl. Phys.* **1974**, *45*, 1456–1457.
40. Chikh, H.; Si-Ahmed, F.; Afir, A.; Pialoux, A. In-situ X-ray Diffraction Study of Alumina α -Al₂O₃ Thermal Behavior. *Int. J. Recent Dev. Eng. Technol.* **2014**, *3*, 137–143.
41. Tonejc, A.; Kosanović, C.; Stubićar, M.; Tonejc, A.; Subotić, B.; Smit, I. Equivalence of ball milling and thermal treatment for phase transitions in the Al₂O₃ system. *J. Alloys Compd.* **1994**, *204*, L1–L3. [[CrossRef](#)]
42. Bodaghi, M.; Mirhabibi, A.; Zolfonun, H.; Tahriri, M.; Karimi, M. Investigation of phase transition of γ -alumina to α -alumina via mechanical milling method. *Phase Transit.* **2008**, *81*, 571–580.

43. Kozawa, T.; Naito, M. Mechanically induced formation of metastable χ - and κ - Al_2O_3 from boehmite. *Adv. Powder Technol.* **2016**, *27*, 935–939.
44. Daraio, D.; Vioria, J.; Ingram, A.; Alexiadis, A.; Stitt, E.H.; Munnoch, A.L.; Marigo, M. Using Discrete Element method (DEM) simulations to reveal the differences in the γ - Al_2O_3 to α - Al_2O_3 mechanically induced phase transformation between a planetary ball mill and an attritor mill. *Miner. Eng.* **2020**, *155*, 106374. [[CrossRef](#)]

Disclaimer/Publisher's Note: The statements, opinions and data contained in all publications are solely those of the individual author(s) and contributor(s) and not of MDPI and/or the editor(s). MDPI and/or the editor(s) disclaim responsibility for any injury to people or property resulting from any ideas, methods, instructions or products referred to in the content.